1-14-92
E-6572

NASA Technical Memorandum 105245

Elevated Temperature Mechanical Behavior of Monolithic and SiC Whisker-Reinforced Silicon Nitrides

Jonathan A. Salem
Lewis Research Center
Cleveland, Ohio

Sung R. Choi
Cleveland State University
Cleveland, Ohio

William A. Sanders
Analex Corporation
Brook Park, Ohio

and

Dennis S. Fox
Lewis Research Center
Cleveland, Ohio

December 1991

NASA

ELEVATED TEMPERATURE MECHANICAL BEHAVIOR OF MONOLITHIC AND SIC WHISKER-REINFORCED SILICON NITRIDES

Jonathan A. Salem
National Aeronautics and Space Administration
Lewis Research Center
Cleveland, Ohio 44135

Sung R. Choi*
Cleveland State University
Cleveland, Ohio 44115

William A. Sanders
Analex Corporation
Brook Park, Ohio 44142

and

Dennis S. Fox
National Aeronautics and Space Administration
Lewis Research Center
Cleveland, Ohio 44135

Abstract

The mechanical behaviors of 30 vol % SiC whisker reinforced silicon nitride and a similar monolithic silicon nitride were measured at several temperatures. Measurements included strength, fracture toughness, crack growth resistance, dynamic fatigue susceptibility, post oxidation strength and creep rate. Strength controlling defects were determined with fractographic analysis. The addition of SiC whiskers to silicon nitride did not substantially improve the strength, fracture toughness, or crack growth resistance. However, the fatigue resistance, post oxidation strength and creep resistance were diminished by the whisker addition.

Introduction

Low reliability and inadequate damage tolerance are the limiting factors in the application of ceramic materials as components in advanced heat engines. Although significant improvement of such mechanical properties have been achieved via processing technology, further improvements are desired. The addition of reinforcing agents to monolithic ceramics, such as SiC whiskers to alumina ceramics, has improved both fast fracture and time dependent properties such as strength, fracture toughness, fatigue and thermal shock (refs. 1 to 7). Unfortunately, the addition of a second phase material, though improving some properties, often degrades other mechanical properties.

The objective of this work was to determine the benefits of whisker addition to silicon nitride, along with the nature and severity of any associated degradation in the properties used in design of high temperature, ceramic engine components. In this study the mechanical properties are described for a monolithic silicon nitride and a 30 vol % SiC whisker-reinforced silicon nitride made from the same powder batch. Although these materials were extensively evaluated previously in terms of fast fracture behavior (refs. 8 and 9) the data is included herein with results of extended time-dependent behavior in order to give the complete property description required for component life prediction.

*NASA Resident Research Associate at Lewis Research Center.

Materials and Test Procedures

Materials

The materials used in this study were based on Garrett GN-10[1] composite and monolithic silicon nitrides. The composite material was developed at Garret Ceramic Components and has been described elsewhere (ref. 10). Briefly, a silicon nitride powder composition was slip cast into 50 mm diameter by 75 mm height billets, glass encapsulated by the ASEA[2] method and hot-isostatically pressed to produce GN-10 monolithic silicon nitride material. Part of the same powder batch was blended with 30 vol % SiC whiskers by ACMC[3] and processed with the same procedures and additives as the monolithic. Densities of the composite and monolithic materials were 3.27 and 3.31 g/cm^3, respectively. Etched microstructures of the materials are shown in figure 1.

Strength

Billets of both composite and monolithic materials were cut to produce flexure test specimens such that the longitudinal axis of the specimens was parallel to the billet height. All faces and bevels of the test specimens were ground with number 320 diamond wheels and the edges were then hand-polished with number 600 grit SiC paper lengthwise to eliminate spurious failures from edge chips. The flexure strength was determined in four-point bending at temperatures from 25 to 1400 °C with a SiC fixture. The specimens measured 2.7 by 4 mm in height and width, respectively. A SiC bend fixture with 20 and 40 mm inner and outer spans, respectively, was used.

The location and nature of failure origins were determined with optical and scanning electron microscopy.

Fracture Toughness

Fracture toughness from room temperature to 1400 °C was determined with the chevron-notch (ref. 11) (CN) method in four-point bending. Specimens measured 3 by 6 mm in width and height and the inner and outer spans were 20 and 40 mm, respectively. Chevron-notch specimens were tested at 0.01 mm/min. The slow stroke rate was used to insure stable crack extension. The fracture toughness was also measured with single-edge-precracked-beam (SEPB) (ref. 12) and indentation strength (IS) (ref. 13) methods at room temperature.

Crack Growth Resistance

The room temperature crack growth resistance was estimated using the indentation strength method proposed by Krause (ref. 14), and from the results of the SEPB fracture toughness tests. Test specimens for indentation strength were 3 by 6 by 25 mm bars with the center of the tensile surface polished and indented with a Vicker's indenter at loads ranging from 49 to 294 N. The subsequent strength tests of the indented samples were conducted in four-point bending with spans of 10 and 18 mm, and a stroke rate of 0.2 mm/min. Three to four specimens were tested at each indentation load. Krause (ref. 14) has shown that R-curve behavior can be evaluated from indentation strength data, assuming that fracture resistance (K_r) is related to the crack length (c) by a power-law relationship. The fracture resistance and the indentation strength (σ_r) relations are expressed

$$K_r = kc^{\tau} \tag{1}$$

$$\sigma_r = \left[k(3+2\tau)/(4\beta)\right]\left[4P\gamma/\left(k(1-2\tau)\right)\right]^{\frac{2\tau-1}{2\tau-3}} \tag{2}$$

where k and τ are constants, γ and β are the dimensionless quantities associated with the residual contact stress and the crack geometry, respectively, and P is the indentation load. When $\tau = 0$, equation (2) reduces to the case of no crack resistance toughening, and equation (1) reduces to $K_r = K_{IC}$. The parameter τ was evaluated from the best-fit slope of the Log σ_r-Log P data and equation (2). The constant k was evaluated from equation (1) with the estimated τ and the fracture toughness obtained from from the SEPB specimens with an average macroscopic crack size of c = 1600 μm.

Fatigue Susceptibility

Dynamic fatigue tests were conducted in ambient air at temperatures of 1100, 1200 and 1300 °C using a fully-articulated four-point bend fixture made from sintered SiC. The inner and outer spans were 20 and 40 mm, respectively.

A preliminary study showed that a loop-shaped load-controlled mode of the test machine[4] gave far better results in testing the specimens than the position-controlled mode (constant cross-head speed). The load-control mode eliminated secondary loads transmitted to the specimen as a result of thermal expansion of the load train members (push rods, grips, and water cooled adaptors, etc.) caused by changes in cooling water temperature and room temperature. This is of particular significance in long duration testing where ambient temperature fluctuations may be difficult to control.

Four loading rates of 2000 N/min to 2 N/min, corresponding to the stressing rates of 2000 MPa/min to 2.0 MPa/min, were applied at temperatures of 1100 and 1300 °C. At 1200 °C only two stressing rates of 2000 and 2 N/min were employed

[1]Garrett Ceramic Components, Allied Signal, Torrance, CA.
[2]ABB Autoclave Systems, Columbus, OH.
[3]Advanced Composite Materials Corp., Greer, SC.
[4]Model 8562, Instron Corp., Canton, MA.

due to the limited number of the specimens. The stressing rate ($\dot{\sigma}$) was calculated using the relation from elementary beam theory

$$\dot{\sigma} = 3(S_o - S_i)\dot{P} / \left[2bh^2\right] \qquad (3)$$

where S_o and S_i are the outer and inner spans of the test fixture, respectively, $\dot{P}$ is the loading rate, and b and h are the specimen width and height, respectively. Three to five specimens were tested at each loading rate. Each specimen was preloaded with 20 N to maintain a good alignment of the test specimen in the fixture. The heating rate of the furnace was 12 °C/min, and each specimen was held at test temperature for 20 min. prior to testing.

For comparison, an additional dynamic fatigue test was carried out with indented specimens at 1100 °C in air. Specimens measuring 2.7 by 4 by 25 mm were indented using a Vicker's microhardness indenter with 98 N such that one of the indentation diagonals was aligned normal to the direction of the applied tensile stress. A four-point bend SiC fixture with spans of 19.0 and 9.5 mm was used to fracture the specimens at loading rates of 4200 to 4.2 N/min, corresponding to the stressing rates of 2000 to 2.0 MPa/min. Three specimens were tested per loading rate. This was considered sufficient in view of the small standard deviation (less than 7 percent) of the mean strength.

The fatigue susceptibility parameters n and B were obtained, respectively, from the slope and intercept of the dynamic fatigue curve of Log σ_f versus Log $\dot{\sigma}$ based on linear regression analysis (ref. 15, 16)

$$\sigma_f^{n+1} = \dot{\sigma} B(n+1)\sigma_i^{n-2} \qquad (4)$$

where $B = 2/[AY^2(n-2)K_{IC}^{n-2}]$, σ_i is the inert strength, and Y is the crack geometry factor. Consequently, the parameter A of the empirical crack velocity equation (ref. 17)

$$V = A'\left[K_I / K_{IC}\right]^n = AK_I^n \qquad (5)$$

was evaluated using equation (4) with appropriate constants. The parameters K_I and K_{IC} are the mode I stress intensity factor and the fracture toughness, respectively, A' and n are the material and environmental constants and $A = A'[K_{IC}]^{-n}$.

Fractographic analysis was conducted using optical and scanning electron microscopy to characterize the nature of failure origins and the mode of crack growth.

Oxidation

Oxidation tests were conducted by heating bend bars at 1000, 1200, or 1400 °C for 500 hr in 100 cm^3/min flowing oxygen. Four-point bend strength of the materials after the 500 hr exposures was determined at 25 °C. Specimens measured 3 by 4 mm in height and width, with load spans of 20 and 40 mm. Five specimens were tested at a crosshead speed of 0.5 mm/min for each exposure temperature. Fractography was conducted with scanning electron microscopy.

Creep

Creep tests were conducted by dead weight loading of 3 by 4 by 50 mm flexure specimens with spans of 19 and 38 mm. Stress levels of 200, 250, 300, and 350 MPa were applied at 1250 °C in air. The displacement measurement system included an LVDT transducer with a 3-point extensometer made of Al_2O_3 gage rods with SiC tips. The SiC tips were in contact with the specimen tensile surface at the center and beneath the inner load points. Strain calculations were made assuming a constant radius of curvature between the inner load points. The simple relation $e_{max} = 4h \times d/S_i^2$ was employed, where e_{max} is the maximum strain in the outer fiber, d is the relative deflection of the bar center with respect to the inner load points, and S_i is the inner span (ref. 18).

Results and Discussion

Strength

Bend strength as a function of temperature for the as-received materials is shown in figure 2. The room temperature strength was σ_i = 698±85 MPa and 732±61 MPa for the composite and monolithic materials, respectively. Weibull modulus of the strength distribution was not available due to the limited number of test specimens (typically less than 10). However, Weibull modulus (m) can be approximated using the formula of $m \approx 1.2/[C.V.]$ as proposed by Ritter et al. (ref. 19), where C.V. is the coefficient of variation of the mean strength. Using this relation together with the obtained values of C.V. for the two materials at room temperature, Weibull moduli of the composite and monolithic are estimated to be $m \approx 9.8$ and 14.4, respectively. Despite the insufficient number of test specimens, the estimated Weibull modulus is in good agreement with the typical range of $m \approx 7$ to 15 commonly observed for sintered silicon nitride materials. It is important to note that a low Weibull modulus suggests nonuniformity and/or inhomogeneity in composition and microstructure of a material.

Examination of the fracture surfaces for both materials showed that most failures originated from surface and subsurface porous regions, coarse grained regions, chunks of silicon nitride and agglomerates. Typical examples of failures are shown in figures 3 and 4. The chunks of silicon nitride were not associated with processing contaminants such as metallic particles (e.g., iron). For both materials, the room temperature strength was retained with little variation up to 1100 °C; however, appreciable strength degradation occurred

above 1200 °C. At 1400 °C, the degradation reached 50 and 45 percent of the room temperature strength of the composite and monolithic materials, respectively. This high temperature strength degradation, particularly at 1400 °C, is believed to be associated with slow crack growth and creep deformation due to the softening of the grain boundaries. A large region of stable crack growth that occurred in a composite specimen at 1300 °C is shown in figure 5.

In general, the average strength of the monolithic material was about 5 to 15 percent higher than the composite. However, in view of the range of experimental error, it can be concluded that the strengths of both composite and monolithic materials are virtually the same, as seen in figure 2. This indicates that the whisker addition to the silicon nitride matrix did not provide any favorable effect on strength.

Fracture Toughness

The results of the fracture toughness measurements from the chevron-notch method are presented in figure 6. The measured fracture toughness for both materials is plotted as a function of test temperature from 25 to 1200 °C. Contrary to the strength behavior, fracture toughness degradation with increasing temperature was not observed for the two materials. Over the test temperature range, the fracture toughness (room temperature K_{IC} = 5.5±0.3 and 5.3±0.3 MPa$\sqrt{m}$ for the composite and monolithic, respectively) remained almost unchanged (within 10 percent), indicating that toughness for both materials is independent of test temperature up to 1200 °C. Also, note the negligibly small difference in toughness values between the two materials. The overall fracture toughness was K_{IC} = 5.7±0.3 MPa$\sqrt{m}$, as indicated by the horizontal line in figure 6.

It should be noted that an unusually high fracture toughness of $K_{IC} \geq 10$ MPa/m was obtained for both materials at the temperature of 1400 °C. This was possibly due to increased plasticity and/or creep deformation associated with the combined effects of high temperature and slow testing speed of 0.01 mm/min, as reported previously (ref. 8). The SEPB method in an inert environment is thought to be a good alternative for measuring fracture toughness at high temperature. However, application of the SEPB at elevated temperatures in air resulted in precrack healing and a measured fracture toughness that depended on heating rate and soak time.

A summary of the fracture toughness evaluated at room temperature with the chevron notch, SEPB, and indentation strength methods is shown in figure 7. The fracture toughness was independent of the test method for both materials. Also, note that there was virtually no difference in fracture toughness between the two materials. The average room temperature fracture toughness was K_{IC} = 5.4±0.2 MPa$\sqrt{m}$, as shown in figure 7. This result implies that crack growth resistance of the materials remains constant regardless of the crack size, for either the micro-crack (indented) or the macro-crack (SEPB and CN) regime. Crack growth resistance as a function of crack size, (R-curve behavior), will be discussed in the next section.

The lack of appreciable difference in fracture toughness between the two materials implies that the whisker addition was ineffective as a toughening mechanism for the current material system. Toughening mechanisms such as crack deflection by the whiskers and pullout of the whiskers have been suggested and observed to be operative for some reinforced ceramics (ref. 20, 21). Fracture surfaces of this composite material exhibited some whisker pullout (fig. 8). However, the number and extent of whisker pullouts are thought to be insufficient to achieve a noticeable gain in fracture toughness. Also, note that many of observable whiskers impressions are aligned parallel to the fracture plane (fig. 8(b)). Proper alignment of whiskers relative to the crack plane (i.e., whisker axis aligned perpendicular to crack plane) is a prerequisite to enhance fracture toughness of the composite material.

Recently, Becher et al. (ref. 22) modeled the toughening behavior of whisker reinforced ceramics based on stress intensity and the energy change introduced by bridging whiskers with some simplifying assumptions. Their resulting expression of toughening contribution (δK) is

$$\delta K = 1/2\left[\left(K_o^2 + Q\right)^{1/2} - K_o\right] \qquad (6)$$

where

$$Q = 2\left(\sigma_f^w\right)^2 r V_f E^c G^m / 3\left(1-\nu^2\right) E^w G^i$$

and where K_o is the matrix toughness, r is the whisker radius, σ_f^w the whisker strength, V_f the volume fraction of whiskers, ν the Poisson's ratio of the composite, and E and G are the Young's modulus and fracture energy, respectively. The superscripts c, w, m, and i denote composite, whisker, matrix, and interface, respectively. For the given whisker (σ_f^w, E^w and V_f) and given matrix conditions, the toughening is strongly dependent on the interface fracture energy G^i. In other words, the interfacial fracture energy must be small so that partial debonding of the whisker along the whisker/matrix interface occurs to form the whisker bridging. In order to obtain a δK = 10 percent increase in toughening from the current composite (V_f = 0.3), the fracture energy ratio of matrix to interface given in equation (6) needs to be $G^m/G^i \approx 6$ for experimental and literature values of $\sigma_f^w \approx 8$ GPa (ref. 23), $r \approx 0.21$ μm, $\nu \approx 0.2$, $E^c \approx 300$ GPa, $E^w \approx 580$ GPa (ref. 23), K_o = 5.4 MPa$\sqrt{m}$, and δK = 0.54 MPa$\sqrt{m}$. To achieve a 50 percent increase in toughening, for example, the ratio G^m/G^i should be increased by factor of 10 from the 10 percent toughened composite system. Controlling the matrix/whisker interface is thus crucial in tailoring the toughness property of the composite materials. However, additional complexities involved with interface surface chemistry, whisker

morphology, pullout length, and thermal expansion mismatches are also known to strongly influence whisker toughening (ref. 24).

R-Curve Behavior

A summary of the fracture parameters τ and k is given in table I. Included in this table is the best-fit slope from the linear regression analysis of Log σ_f versus Log P for each material. The predicted fracture resistance curve based on equation (1) is presented in figure 9. Both composite and monolithic materials exhibit negligibly small toughening exponents of $\tau \leq 0.04$ (i.e., no R-curve).

The flat R-curve behavior of the composite material was also observed from the fracture toughness values determined using SEPB specimens at room temperature. Figure 10 shows a plot of fracture toughness as a function of normalized crack size a/W, where a is the precrack size and W is the specimen height. The different crack sizes were obtained by varying the applied indentation load, which not only triggers crack pop-in, but determines the precracking load and precrack size (ref. 12). It can be seen from figure 10 that the fracture toughness is insensitive to the precrack size since most values are within ±1.0 standard deviation of the mean (5.2± 0.4 MPa$\sqrt{m}$), in agreement with the result obtained from the indentation method.

This flat R-curve behavior of the composite material indicates that the whisker addition to the silicon nitride matrix did not result in any favorable effect on crack growth resistance. This result is consistent with the previous work for another 30 vol % SiC whisker/silicon nitride composite material where the toughening exponent was determined to be $\tau = 0.03$ (ref. 25). Rising R-curve behavior has been observed for ceramic materials such as Al_2O_3 ($\tau = 0.13$) (ref. 14), 25 wt % SiC whisker reinforced Al_2O_3's ($\tau = 0.08$) (ref. 26), and *in situ* toughened silicon nitrides ($\tau = 0.1$-0.2) (ref. 27 to 29).

Fatigue Susceptibility

A summary of the dynamic fatigue results is presented in table II. Note that the time to failure at the lowest stressing rate ($\dot{\sigma}$ = 2 MPa/min) was less than 6 hr, and that this duration of time was assumed insufficient to induce any cavitation in the tensile surface and a resulting shift of the neutral axis toward the compression side for either material, even if the materials exhibited limited creep deformation at high temperature. Therefore, since $\dot{P}$ was constant during testing, the corresponding stressing rate ($\dot{\sigma}$) was assumed constant (eq. (3)).

Table III summarizes the parameters n, B and A evaluated from the experimental data based on equations (3) and (4). The values of inert strength (σ_i) and fracture toughness were taken from the previous results: for the composite material σ_i = 698 MPa and K_{IC} = 5.7 MPa$\sqrt{m}$; whereas for the monolithic σ_i = 732 MPa and K_{IC} = 5.7 MPa$\sqrt{m}$. The crack geometry factor was taken to be Y = 1.13, as the strength controlling flaws were observed to be half penny-shaped in configuration, as described at the end of this section. The parameters B and A were not estimated for the indented specimens due to an insufficient number of specimens to determine the strength (σ_i) in the indented and annealed condition.

Figure 11 shows the dynamic fatigue results of the as-received composite specimens. The decrease in fatigue strength with decreasing stressing rate indicates that fatigue (slow crack growth) occurred. The fatigue susceptibility parameter n decreased rapidly from 88.1 to 20.1 as the corresponding temperature increased from 1100 to 1300 °C, which indicates that fatigue susceptibility increases very rapidly with increasing temperature. It is also important to note that a transition in the dynamic fatigue curve occurs at the lowest stressing rate of $\dot{\sigma}$ = 2.0 MPa/min at 1300 °C, resulting in a very low value of n = 5.8. The transition was attributed to creep deformation enhanced by both the high temperature and very slow stressing rate. Appreciable creep strain was observed for the specimens tested at this condition. It should be emphasized that such transition should be taken into account when reliability and lifetime prediction (design methodology) are made for structural components, as mentioned by Fett and Munz (ref. 30). This requires a more in-depth understanding of both slow crack growth and creep behaviors, particularly under a constant loading rate condition.

The results of dynamic fatigue tests of the monolithic material are presented in figure 12. As seen for the composite material (fig. 11), the fatigue strength decreases with both increasing stress rate and increasing temperature. However, the fatigue parameter n for the monolithic decreased monotonically from 50.8 to 40.4 with increasing temperature from 1100 to 1300 °C. This behavior contrasted to that of the composite material which exhibited a transition in the fatigue curve at 1300 °C due to creep. Although the monolithic material exhibited creep at elevated temperatures, it did so less than the composite material, as shown in figure 13.

Results of dynamic fatigue tests of the indented composite specimens at 1100 °C are presented in figure 14. For comparison the fatigue strength data of the as-received specimens is included. The parameter (n = 50.8) for the indented specimens is lower than that (n = 88.1) obtained from the as-received specimens. In other words, the fatigue resistance of inherent flaws is greater than that of artificial flaws produced by indentation. This indicates that the fatigue behavior of well-defined cracks is somewhat different from that of the inherent flaws, implying that the two flaw systems may not be identical to each other. It is thought that the inherent flaws either take longer to initiate crack growth or have a more ill-defined crack configuration as compared to the indent crack, thereby resulting in a more deviant crack propagation behavior.

Typical examples of the fracture surfaces for the specimens tested at 1300 °C with stressing rates of 2.0 and

2000 MPa/min are shown in figures 15(a) and (b). Note the difference in the size of the cracks for the different stressing rates. Figure 15(c) shows a typical fracture surface and associated pullout of some of the whiskers.

Based on these dynamic fatigue results, it can be concluded that whisker addition to monolithic silicon nitride deteriorates the inherent fatigue resistance. This contrasts with results of strength, fracture toughness and crack growth resistances described earlier, for which no appreciable differences were found between the two materials.

Oxidation

Results from x-ray diffraction of the oxidized surfaces are given in table IV. Silica was present on the surfaces in the form of α-cristobalite after the 1000 and 1200 °C exposures. The higher temperature form of tridymite was present on the 1400 °C samples. Silicon carbide was not detected on the surface of SiC whisker reinforced silicon nitride after 1400 °C exposure.

Room temperature bend strength results of oxidized specimens are shown in figure 16 and table V. A summary of the nature of the origins is compiled in table V.

In the composite specimens oxidized at 1000 °C , areas of volume porosity 20 to 40 μm in diameter acted as fracture origins. These processing flaws were much larger than the surface pores (5 to 10 μm) that acted as origins in the 1000 °C monolithic samples. Fractography did not explain the apparent increase in strength of composite silicon nitride after exposure to 1400 °C versus 1200 °C. Surface flaw size was approximately 30 to 50 μm for all samples after exposure at both of these temperatures.

In summary, the monolithic silicon nitride material retained its original room temperature strength after 500 hr of oxidation at temperatures up to 1200 °C, but lost 41 percent of that value after exposure at 1400 °C. By comparison, the composite material retained its original room temperature strength after 500 hr at 1000 °C, but lost 37 percent of that strength after exposure at 1200 °C. Fracture originated primarily at surface pores or surface oxidation pits. Volume pores dominated only in the composite silicon nitride after 1000 °C exposure.

It is concluded that the composite silicon nitride exhibited no performance gain over monolithic silicon nitride in this series of tests.

Creep

Creep strain as a function of time at 350 MPa is shown in figure 17. It should be noted that the neutral axis was not assumed to shift toward the compression side during the creep deformation. The resulting steady state creep rate, based on the equation

$$\dot{\varepsilon} = \alpha\sigma^{N} \qquad (7)$$

is illustrated as a function of applied stress in figure 18. The apparent strain and creep rates were substantially higher for the composite material. The monolithic material exhibited a creep parameter, N = 0.99, typical of values given in the literature for silicon nitrides. The composite material, however, exhibited a much higher parameter, N = 5.61, indicating a poor resistance to creep at 1250 °C. It has been reported by Nixon et al. (ref. 31) that SiC whiskers in a silicon nitride matrix did not directly contribute to the kinetics of compressive creep. However, the addition of SiO_2 on the surfaces of some whiskers did enhance compressive creep, implying that whisker purity is significant to creep. The amorphous grain boundary phase ultimately controlled creep by grain boundary sliding.

Conclusions

The monolithic material exhibited very good fatigue resistance and reasonable strength, Weibull modulus, fracture toughness and creep resistance as compared to other available monolithic silicon nitrides. The addition of 30 vol % SiC whiskers to the monolithic silicon nitride did not substantially improve the strength, fracture toughness, or crack growth resistance. However, the whisker addition did deteriorate the fatigue, creep, and oxidation resistance inherent to the monolithic material. The deterioration may have been due to the addition of silica via the whiskers and concurrent development of less refractory grain boundary phases. At present, improvements in fracture toughness and crack growth resistance of silicon nitride may be better attained via *in situ* toughening.

Acknowledgement

The authors would like to acknowledge Oak Ridge National Laboratory for funding this research under the CTAHE Project, DE-AI05-87OR21749.

References

1. Becher, P.F.; and Wei, G.C.: Toughening Behavior in SiC-Whisker-Reinforced Alumina. J. Am. Ceram. Soc., vol. 67, no. 12, 1984, pp. c267–c269.
2. Wei, G.C.; and Becher, P. F.: Development of SiC-Whisker-Reinforced Ceramics. Am. Ceram. Soc. Bull. vol. 64, no.2, 1985, pp. 298–304.
3. Homeny, J.; Vaughn, W.L.; and Ferber, M.K.: Processing and Mechanical Properties of SiC-Whisker-Al_2O_3-Matrix Composites. Am. Ceram. Soc. Bull., vol. 66, no. 2, 1987, pp. 333–338.
4. Iio, S., et al: Mechanical Properties of Alumina/Silicon Carbide Whisker Composites. J. Am. Ceram. Soc., vol. 72, no. 10, 1989, pp. 1880–1884.

5. Tiegs, T.N.; and Becher, P.F.: Thermal Shock Behavior of an Alumina-SiC Whisker Composite. J. Am. Ceram. Soc., vol. 70, 1987, pp. c109–c111.
6. Becher, P.F., et al.: Elevated-Temperature Delayed Failure of Alumina Reinforced with 20 vol % Silicon Carbide Whiskers. J. Am. Ceram. Soc., vol. 73, no. 1, 1990, pp. 91–96.
7. Tiegs, T.N.;and Becher, P.F.: Whisker-Reinforced Ceramic Composites. Tailoring Mutiphase and Composite Ceramics. Mater. Sci. Res. Vol. 20, R.E. Tressler, et al., eds., Plenum Press, New York, 1986, pp. 639–647.
8. Salem, J.A.: Strength and Toughness of Monolithic and Composite Silicon Nitrides. NASA TM–102423, 1990.
9. Choi, S.R.; and Salem, J.A.: Strength, Toughness, and R-Curve Behaviors of SiC Whisker-Reinforced Si_3N_4 With Reference to Monolithic Si_3N_4. J. Mater. Sci., 1991, to be published.
10. Yeh, H., et al.: "Processing and Mechanical Behavior of Whisker-Toughened Silicon Nitride," Proceedings of the 28th Annual Automotive Technology Development Contractors' Coordination Meeting, SAE, 1990, pp. 255–259.
11. Munz, D.; Bubsey, R.T.; and Shannon, Jr., J.L.: Fracture Toughness Determination of Al_2O_3 Using Four-Point-Bend Specimens with Straight Through and Chevron-Notches. J. Am. Ceram. Soc., vol. 63, no. 5-6, 1980, pp. 300–305.
12. Nose, T.; and Fujii, T.: Evaluation of Fracture Toughness for Ceramic Materials by a Single-Edge-Precracked-Beam Method. J. Am. Ceram. Soc., vol. 71, no. 5, 1988, pp. 328–333.
13. Chantikul, P., et al.: A Critical Evaluation of Indentation Techniques for Measuring Fracture Toughness: II, Strength Method. J. Am. Ceram. Soc., vol. 64, no. 9, 1981, pp. 539–543.
14. Krause, R.F.: Rising Fracture Toughness from the Bending Strength of Indented Alumina Beams. J. Am. Ceram. Soc., vol. 71, no. 5, 1988, pp. 338–343.
15. Evans, A.G.: Slow Crack Growth in Brittle Materials Under Dynamic Loading Conditions. Int. J. Fract., vol. 10, 1974, pp. 251–259.
16. Ritter, J.E.: Engineering Design and Fatigue Failure of Brittle Materials. Fracture Mechanics of Ceramics, R.C. Bradt, et al., eds., Plenum Press, NY, Vol. 4, 1978, pp. 667–686.
17. Evans, A.G.; and Wiederhorn, S.M.: Proof Testing of Ceramic Materials-An Analytical Basis for Failure Prediction. Int. J. Fract., vol. 10, 1974, pp. 379–392.
18. Hollenberg, G.W.; Terwilliger, G.R.; and Gordon, R.S.: Calculation of Stresses and Strains in Four-Point Bending Creep Tests. J. Am. Ceram. Soc., vol. 54, no. 4, 1971, pp. 196–199.
19. Ritter, J.E.; Bandyopadhyay, N.; and Jakus, K.: Statistical Reproducibility of the Dynamic and Static Fatigue Experiments. Am. Ceram. Soc. Bull. vol. 60, no. 8, 1981, pp. 798–804.
20. Becher, P.F.; and Wei, G. C.: Toughening Behavior in SiC-Whisker-Reinforced Alumina. J. Am. Ceram. Soc., vol. 67, no. 12, 1984, pp. c267–c269.
21. Becher, P.F., et al.: Toughening Behavior in Whisker Reinforced Ceramic Matrix Composites. J. Am. Ceram. Soc. vol. 71, no. 12, 1988, pp. 1050–1061.
22. Petrovic, J.J., et al.: Tensile Mechanical Properties of SiC Whiskers. J. Mater. Sci. vol. 20, no. 4, 1985, pp. 1167–11.
23. Homeny, J.; Vaughn, W.L.; and Ferber, M.K.: Silicon Carbide Whisker Alumina Matrix Composites—Effect of Whisker Surface Treatment on Fracture Toughness. J. Am. Ceram. Soc. vol. 73, no. 2, 1990, pp. 394–402.
24. Choi, S.R.; and Salem, J.: Strength and Fracture Toughness Properties of Whisker-Reinforced Silicon Nitride Matrix Composite and Monolithic Silicon Nitride. Symposium on Composites, Am. Ceram. Soc., Ceram. Trans., 1990, Ed. M. Sacks, pp. 741–748.
25. Krause, R.F.; Fuller, E.R.; and Rhodes, J.F.: Fracture Resistance Behavior of Silicon Carbide Whisker-Reinforced Alumina Composites With Different Porosities. J. Am. Ceram. Soc. vol. 73, no. 3, 1990, pp. 559–566.
26. Ritter, J.E., et al.: Effect of Microstructure on the Erosion and Impact Damage of Sintered Silicon Nitride. J. Mater. Sci., vol. 26, 1991, pp. 5543–5546.
27. Li, C.W.; and Yamanis, J.: Super-Tough Silicon Nitride With R-Curve Behavior. Ceram. Eng. Sci. Proc. vol. 10, no. 7–8, 1989, pp. 632–645.
28. Salem, J.A., et al.: Mechanical Behavior and Failure Phenomenon of an *In Situ*-Toughened Silicon Nitride. NASA TM–103741, 1991. (To be published J. Mater. Sci. Vol. 27, 1992).
29. Fett, T.; and Munz, D.: Lifetime Prediction for Hot-Pressed Silicon Nitride at High Temperatures. Methods for Assessing the Structural Reliability of Brittle Materials, ASTM-STP-844, S.W. Freiman and C.M. Hudson, eds., American Society for Testing and Materials, Philadelphia, 1984, pp. 154–176.
30. Nixon, R.D., et al.: Steady-State Creep of Hot-Pressed SiC Whisker Reinforced Silicon Nitride. Compos. Sci. Technol. vol. 37, no. 1-3, 1990, pp. 313–328.

TABLE I.—SUMMARY OF FRACTURE RESISTANCE PARAMETERS FOR MONOLITHIC AND 30 VOL % SIC *WHISKER-REINFORCED SILICON NITRIDES*

Material	Best-fit slope in Log σ_r-Log P curve[a]	Fracture resistance, τ	Parameters, k
Monolithic	-0.30 [b](0.30)	0.04 (0.01)	6.77
Composite	-0.34 (0.04)	0	5.18

[a]The units are in MPa for σ_r, and N for P.
[b]The parenthesis indicates 1.0 standard deviation.
The units are in MPa$\sqrt{m}$ for K_r, and meter for c in Eq. (2).

TABLE II.—SUMMARY OF DYNAMIC FATIGUE RESULTS OF MONOLITHIC AND 30 VOL % SIC WHISKER-REINFORCED SILICON NITRIDES

Temperature, °C	Specimen condition	Stressing rate, $\dot{\sigma}$ (MPa/min)	Composite		Monolithic	
			Number of specimens	Fracture strength σ_f (MPa)	Number of specimens	Fracture strength σ_f (MPa)
1100	As-received	2	5	598.9 [a](63.1)	3	609.2 (35.1)
1100	As-received	20	5	584.5 (82.0)	4	649.0 (45.3)
1100	As-received	200	5	615.9 (54.8)	3	675.3 (41.8)
1100	As-received	2000	5	641.5 (33.8)	4	697.4 (5.1)
1200	As-received	2	4	463.0 (106.4)	3	537.2 (48.4)
1200	As-received	2000	4	558.9 (19.5)	4	621.5 (63.4)
1300	As-received	2	4	318.0 (14.1)	4	513.3 (49.3)
1300	As-received	20	3	445.2 (44.2)	4	523.3 (47.3)
1300	As-received	200	3	487.6 (48.5)	4	596.4 (75.1)
1300	As-received	2000	4	553.9 (38.0)	4	591.4 (21.0)
1100	Indented[b]	2	3	351.4 (4.8)	-	--------
1100	Indented	20	3	353.1 (11.3)	-	--------
1100	Indented	200	3	372.4 (11.1)	-	--------
1100	Indented	2000	3	400.5 (26.9)	-	--------

[a]The numbers in parenthesis indicate 1.0 standard deviation.
[b]Indent load applied to the specimens was 98 N.

TABLE III.—SUMMARY OF FATIGUE PARAMETERS OF MONOLITHIC AND 30 VOL % SIC WHISKER-REINFORCED SILICON NITRIDES

Fatigue parameter	Temperature, °C					
	1100		1200		1300	
	Comp	Mono	Comp	Mono	Comp	Mono
n	88.1	50.8	35.7	46.4	[a]20.1/[b]5.8	40.4
Ln B, MPa^2 min	-1.0219	6.0924	0.2809	0.5762	3.9784/11.6921	0.4346
Ln A, m/min	-151.3	-93.51	-61.4	-86.1	-39.6/-19.1	-75.6

[a]Evaluation based on the stressing rates of 2000, 200 and 20 MPa/min.
[b]Evaluation based on the stressing rates of 20 and 2 MPa/min.

TABLE IV.—X-RAY DIFFRACTION RESULTS

Sample	Exposure temperature, 500 hr	Phases present
Composite Si_3N_4	1000 °C	β-Si_3N_4, α-Si_3N_4[a] α-Cristobalite
Monolithic Si_3N_4	1000 °C	β-Si_3N_4, α-Cristobalite
Composite Si_3N_4	1200 °C	β-Si_3N_4, α-Si_3N_4[1], SiC, α-Cristobalite[1]
Monolithic Si_3N_4	1200 °C	β-Si_3N_4, α-Cristobalite[1]
Composite Si_3N_4	1400 °C	β-Si_3N_4, α-Cristobalite, Tridymite
Monolithic Si_3N_4	1400 °C	β-Si_3N_4, α-Cristobalite, Tridymite

[a]Denotes minor phase.

TABLE V.—AVERAGE POST OXIDATION STRENGTH AND NATURE OF FAILURE ORIGINS (ROOM TEMPERATURE 4-POINT BEND)

Sample	Exposure temperature	Flaw type[a]	Number of occurences	Strength, MPa
Composite Si_3N_4	1000 °C	VP	4	711 [b](87)
		SP	1	
Monolithic Si_3N_4	1000 °C	SP	4	866 (60)
		ND	1	
Composite Si_3N_4	1200 °C	SP	4	447 (28)
		VP	1	
Monolithic Si_3N_4	1200 °C	VP	1	770 (53)
		VG	1	
		SG	1	
		ND	2	
Composite Si_3N_4	1400 °C	SP	5	555 (73)
Monolithic Si_3N_4	1400 °C	SP	3	453 (36)
		VP	2	

[a]Surface grain (SG); surface pore (SP); volume grain (VG); volume pore (VP); nature not determined (ND).

[b]The numbers in parenthesis indicate 1.0 standard deviation.

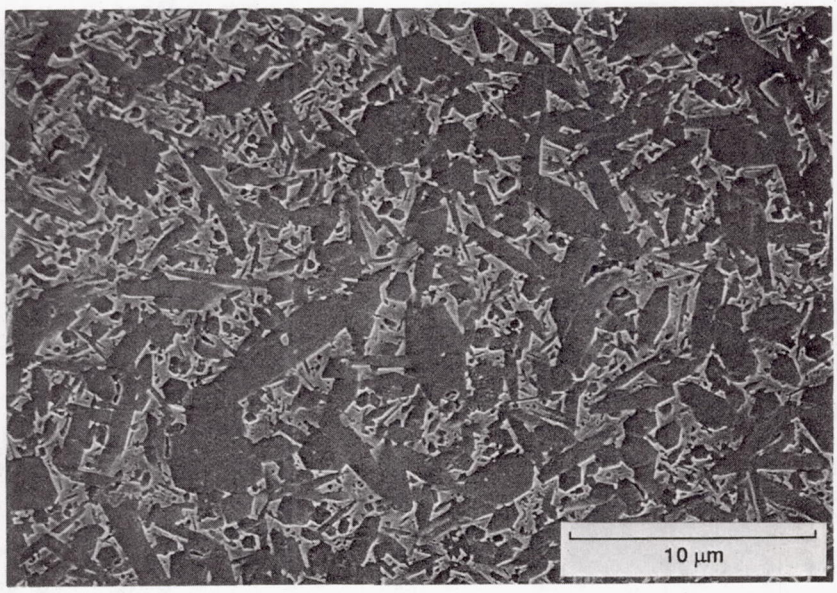

(a) Si_3N_4.

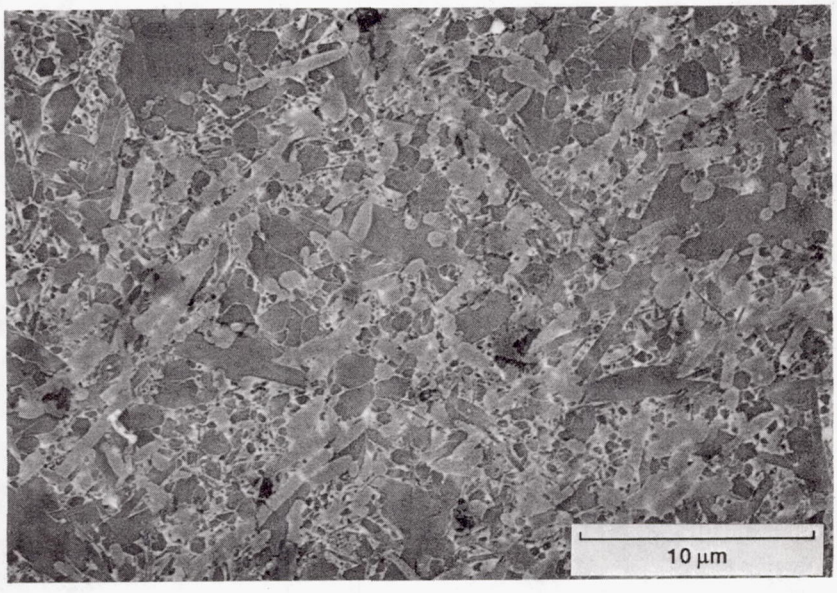

(b) SiC_w/Si_3N_4.

Figure 1.—Etched microstructures: darkest regions are Si_3N_4, grey regions are SiC whiskers and light regions are intergranular phases.

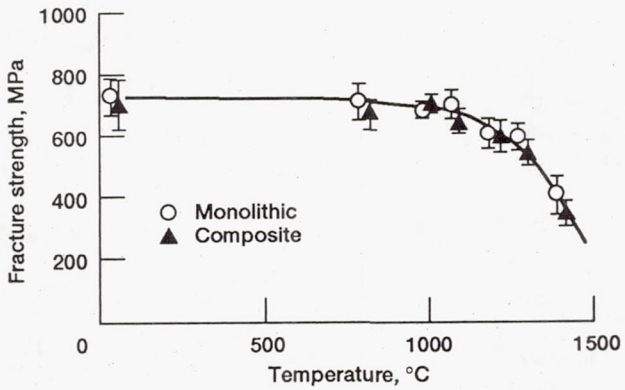

Figure 2.—As-received strength of monolithic and composite silicon nitride as a function of temperature in air. Error bar indicates ± 1.0 standard deviation.

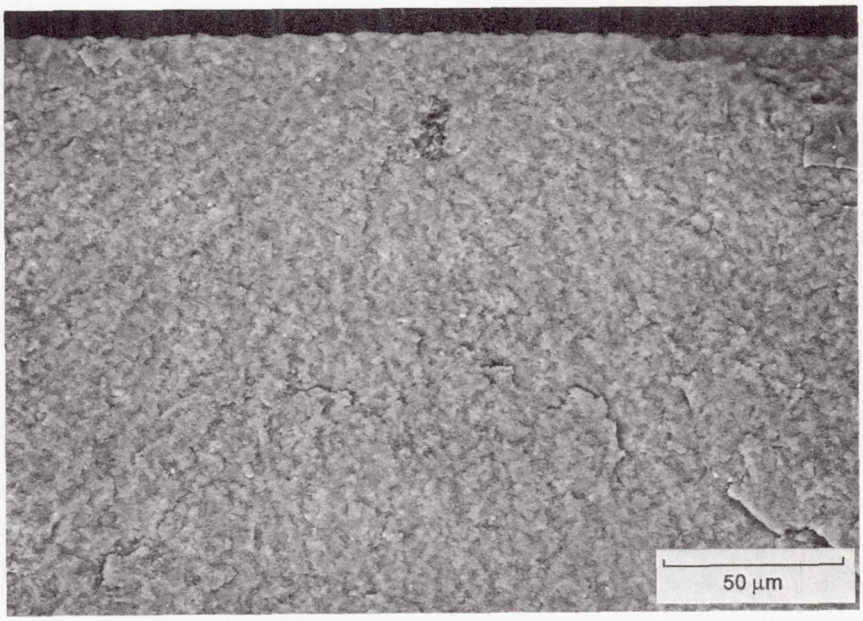

(a) Porosity.

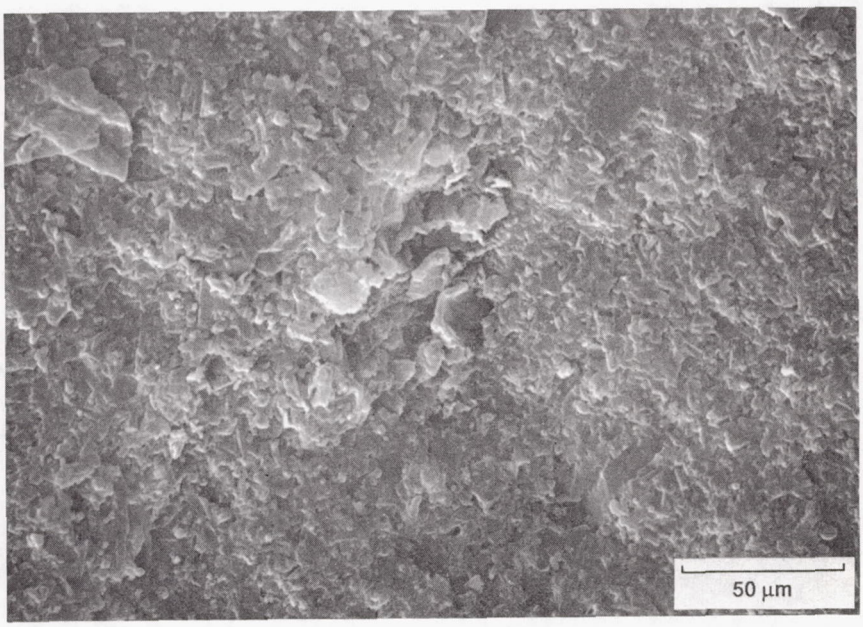

(b) Detail of (a).

Figure 3.—Monolithic fracture origins.

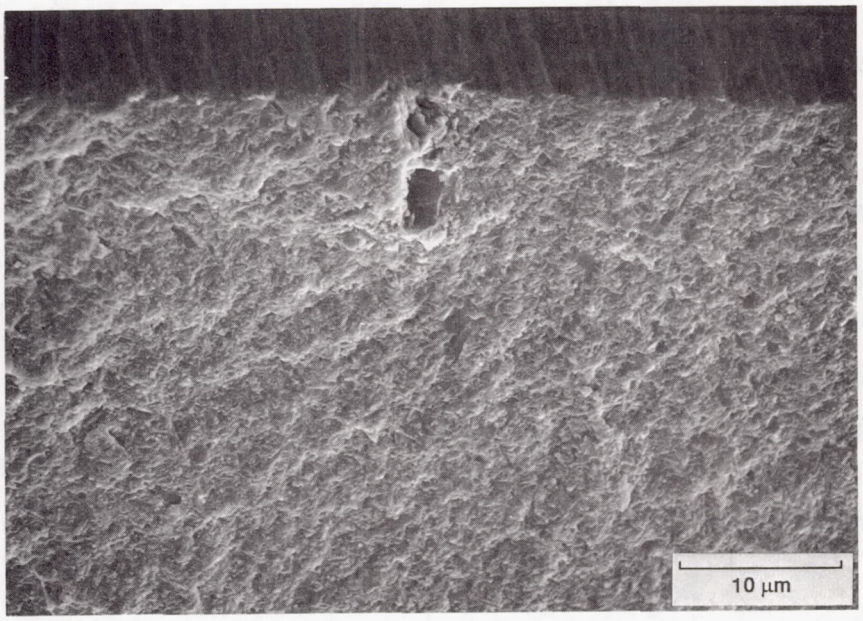

(c) Coarse grain and porosity.

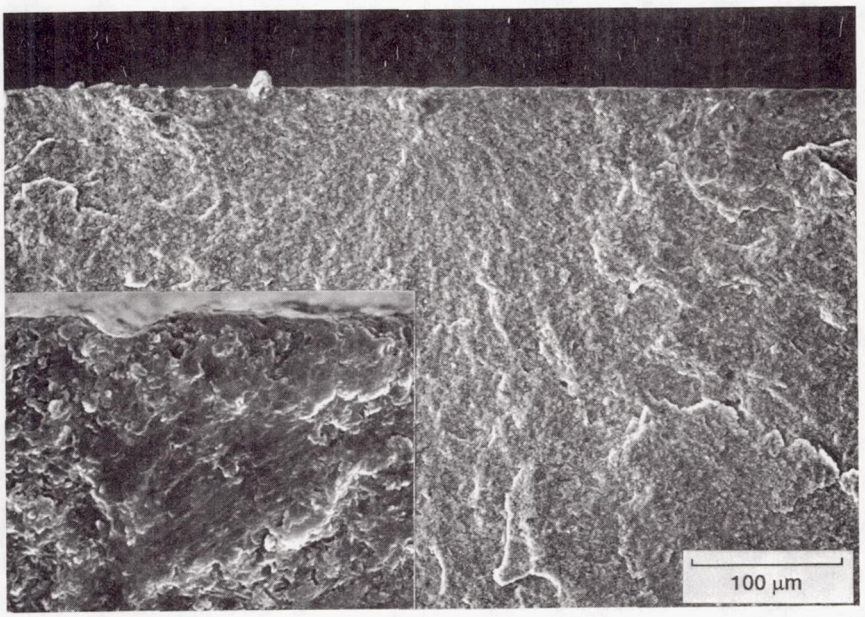

(d) Dense Si_3N_4 chunk with detail shown in inset.

Figure 3.—Concluded.

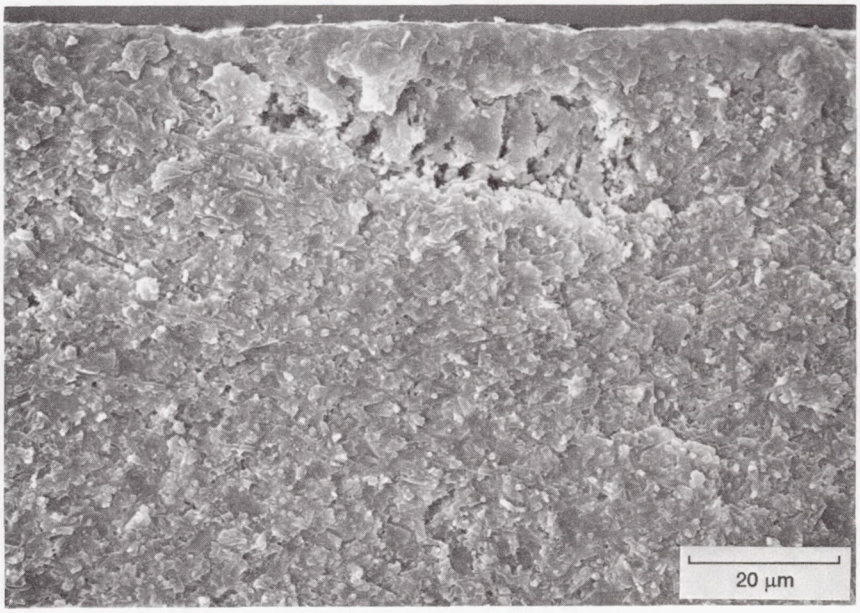

(a) Porous region.

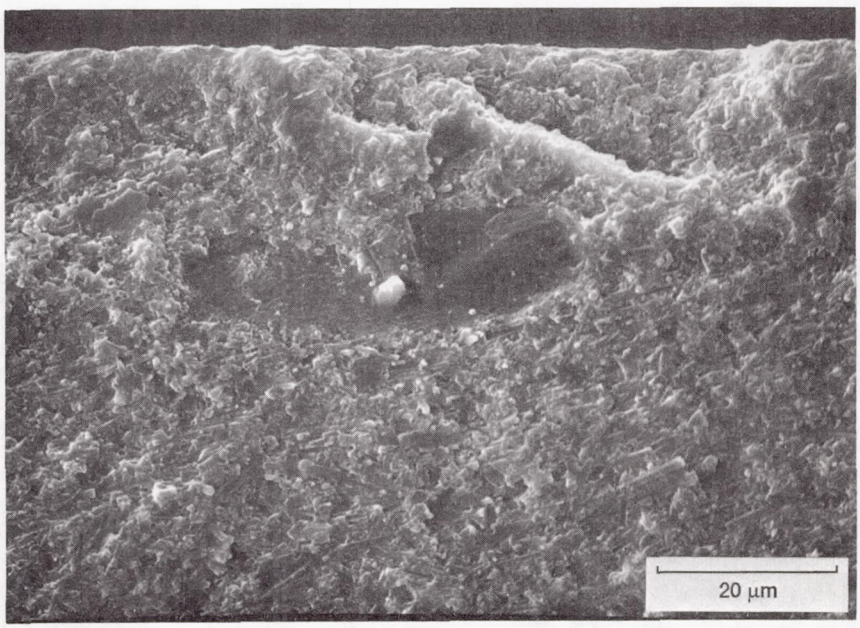

(b) Coarse grain.

Figure 4.—Composite fracture origins.

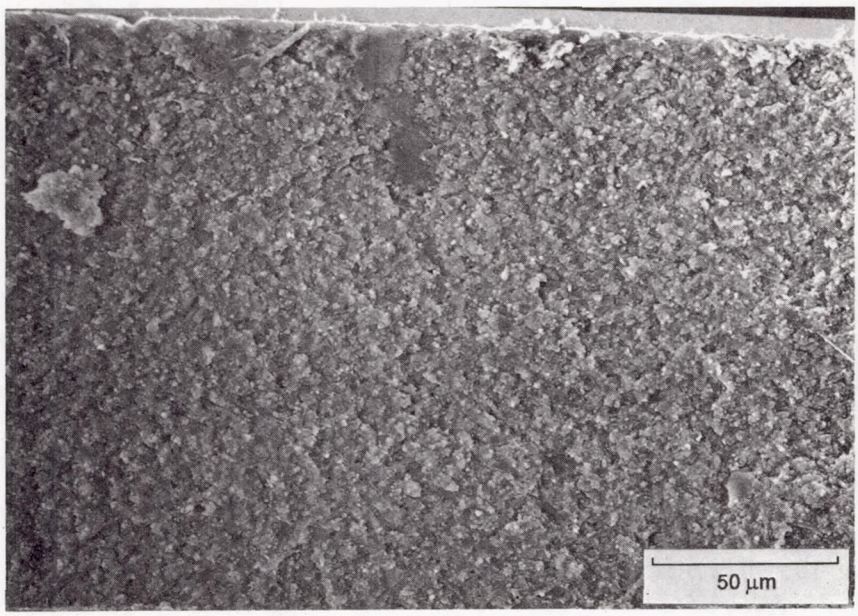

(c) Glassy patch associated with coarse grain.

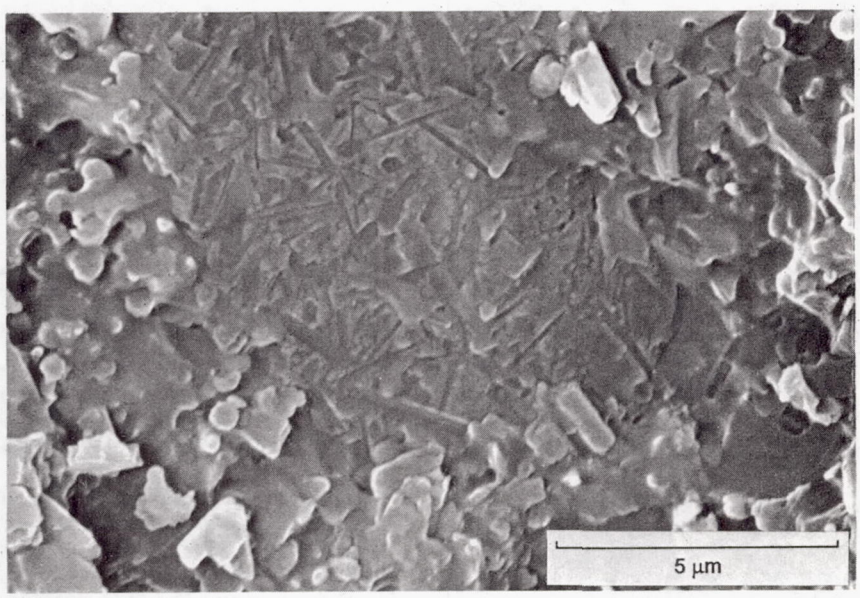

(d) Detail of (c).

Figure 4.—Concluded.

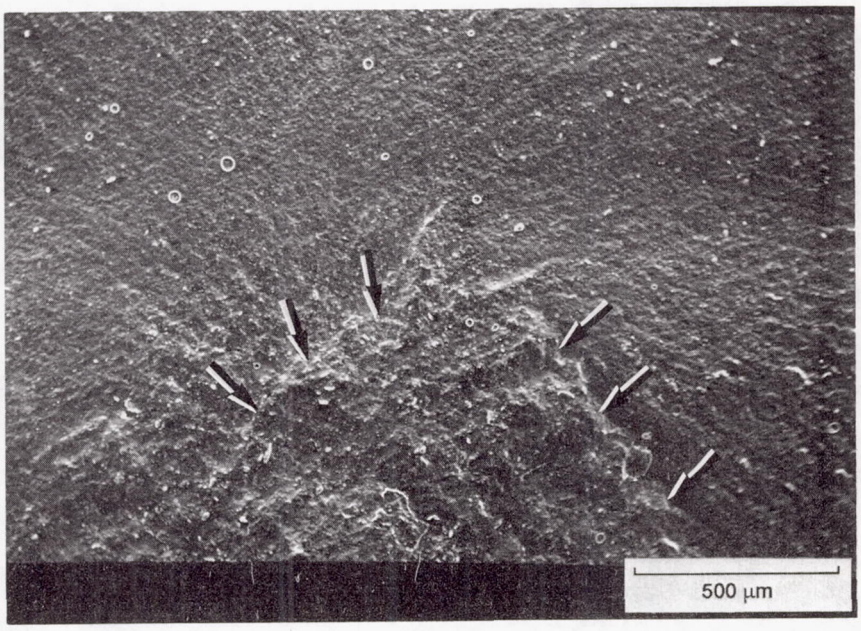

Figure 5.—Crack growth region developed during strength testing of a composite specimen at 1400 °C. Failure occurred at 329 MPa.

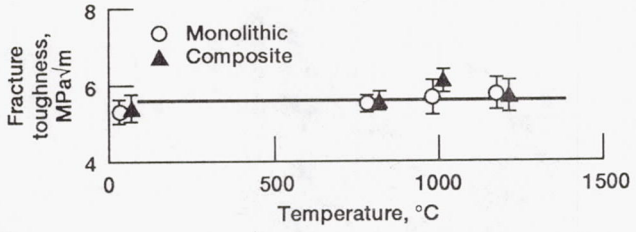

Figure 6.—Chevron notch fracture toughness of composite and monolithic materials as a function of temperature in air. The horizontal line represents an average toughness of 5.7 MPa√m ± 0.3 for all data. Error bar indicates ± 1.0 standard deviation.

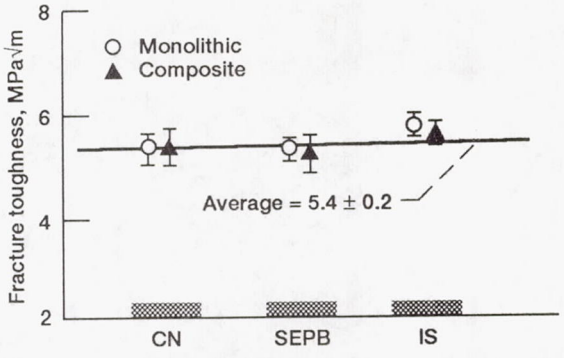

Figure 7.—Room temperature fracture toughness of composite and monolithic materials evaluated from the chevron-notch (CN), Single-Edge-Precracked-Beam (SEPB) and indentation strength (IS) methods. An average value of 5.4 MPa√m ± 0.2 was obtained for all data. Error bar indicates ± 1.0 standard deviation.

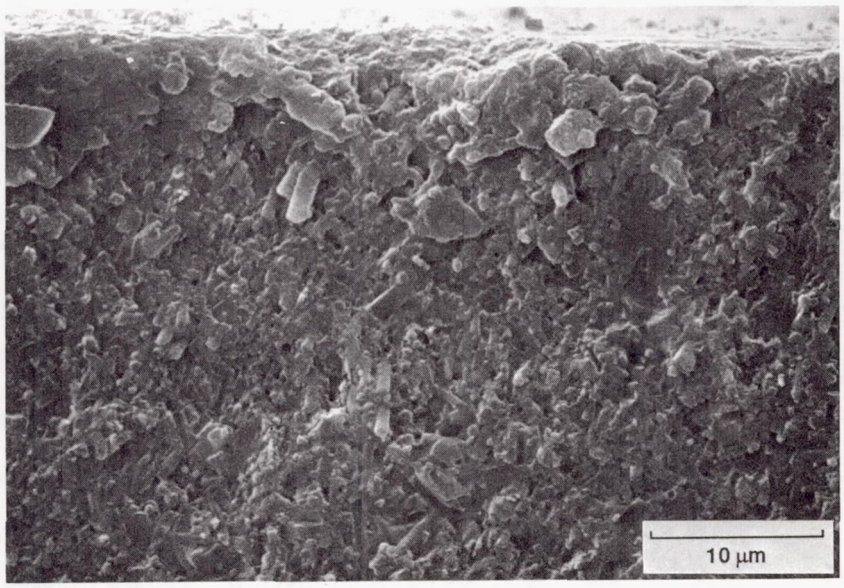

(a) Whisker pullout.

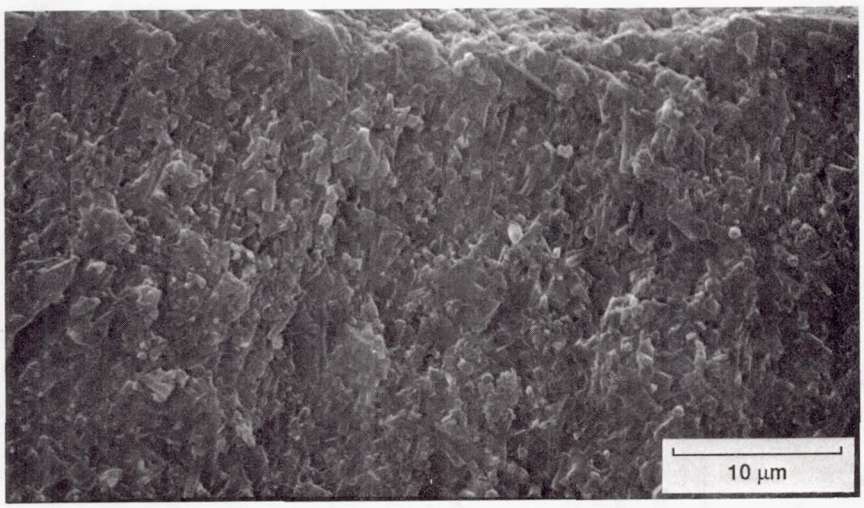

(b) Whisker impressions oriented parallel to the fracture surface.

Figure 8.—Fracture surfaces of the composite material.

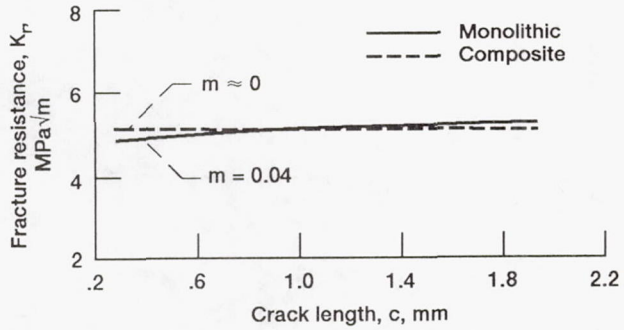

Figure 9.—Predicted fracture resistance curves for composite and monolithic materials.

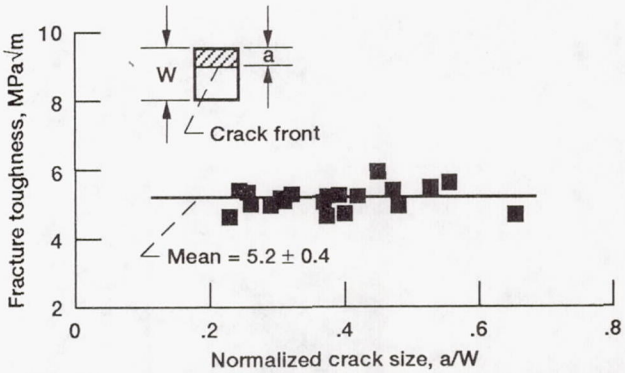

Figure 10.—Fracture toughness of the composite material as a function of normalized precrack length (a/W) measured with SEPB specimens at 25 °C.

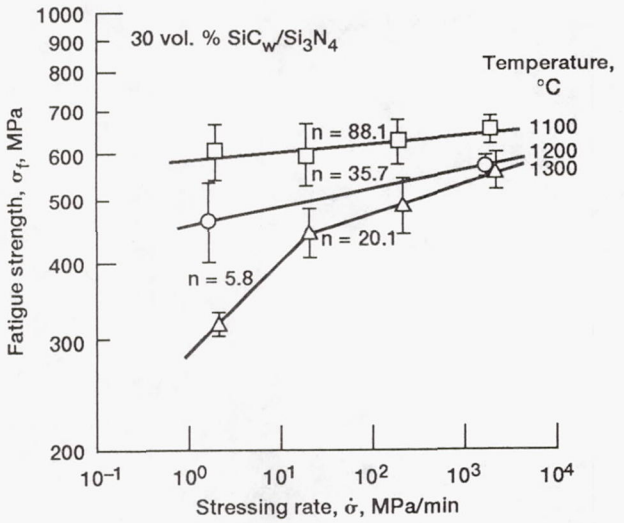

Figure 11.—Dynamic fatigue data for the composite material (as-received condition) in ambient air. Error bar indicates ± 1.0 standard deviation.

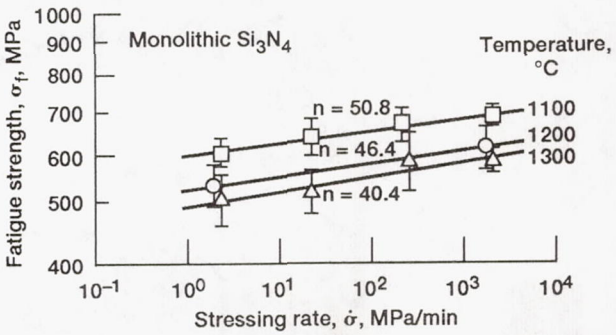

Figure 12.—Dynamic fatigue data for monolithic silicon nitride material (as-received condition) in ambient air.

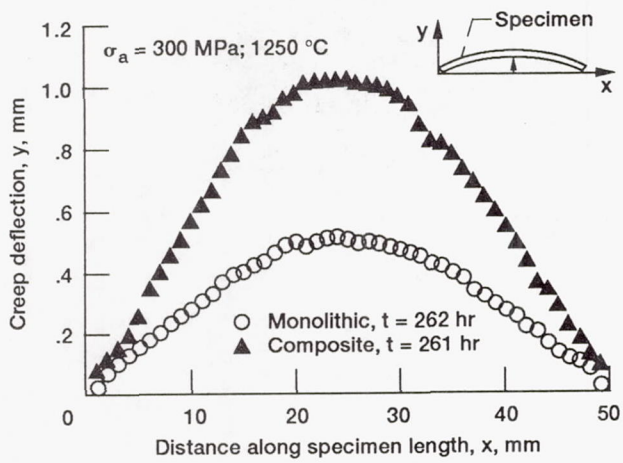

Figure 13.—Creep deformation curves for composite and monolithic specimens subjected to 300 MPa for 260 hr at 1250 °C.

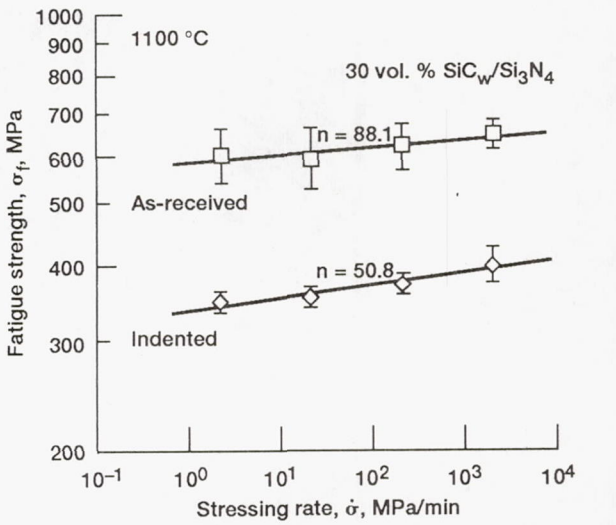

Figure 14.—Dynamic fatigue data for indented composite specimens in ambient air. The fatigue data for as-received specimens is included for comparison.

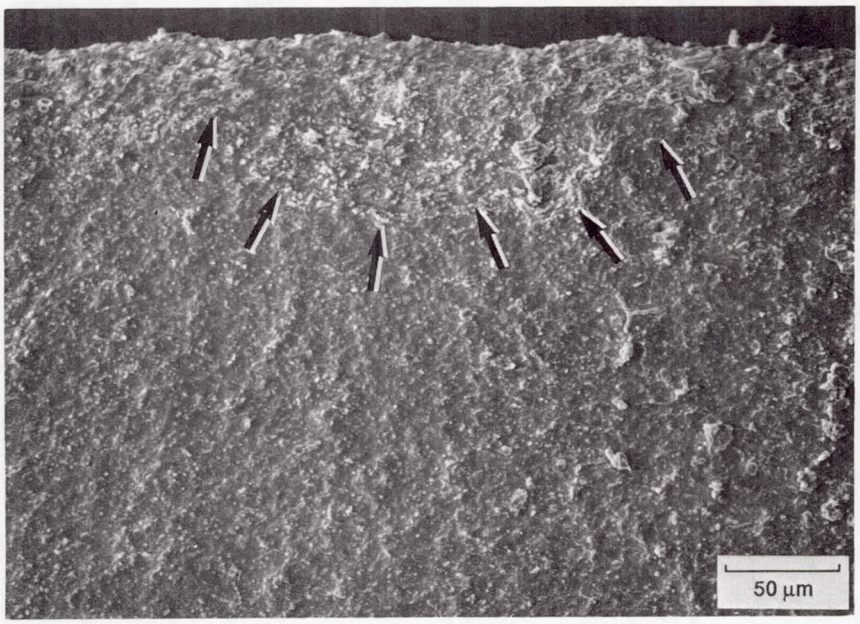

(a) Slow crack growth region for $\dot{\sigma}$ = 2000 MPa/min at 1300 °C. Failure occurred at 514 MPa.

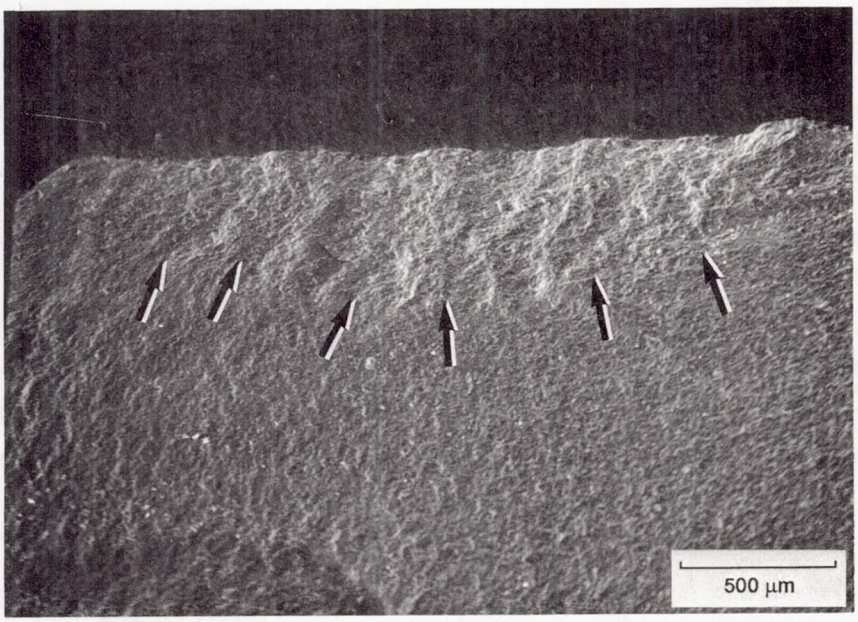

(b) Slow crack growth region for $\dot{\sigma}$ = 2 MPa/min at 1300 °C. Failure occurred at 330 MPa.

Figure 15.—Fracture surfaces of composite specimens tested with high and low stressing rates.

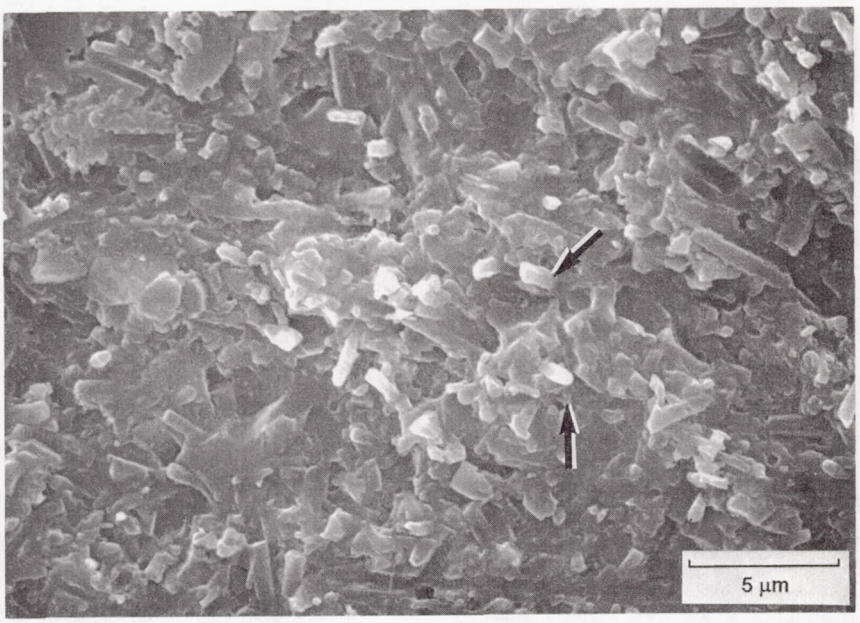

(c) Whisker pullout in slow crack growth region of specimen tested at 1200 °C with $\dot{\sigma}$ = 2 MPa/min. Failure occurred at 370 MPa.

Figure 15.—Concluded.

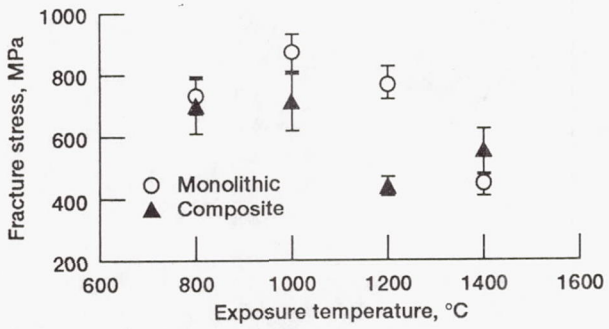

Figure 16.—Room temperature four-point bend strength of monolithic and composite materials after 500 hr exposure in flowing oxygen at 1000, 1200, and 1400 °C. Error bar indicates ± 1.0 standard deviation.

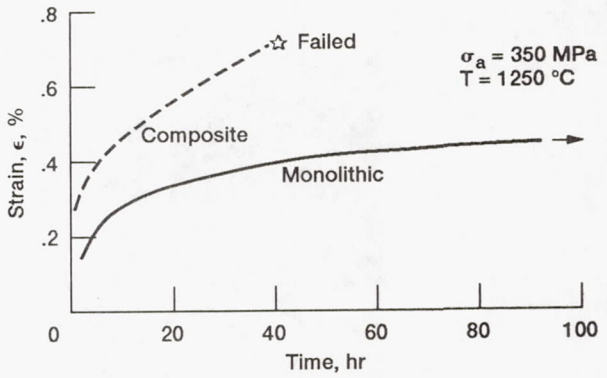

Figure 17.—Creep strain as a function of time at 1250 °C and 350 MPa.

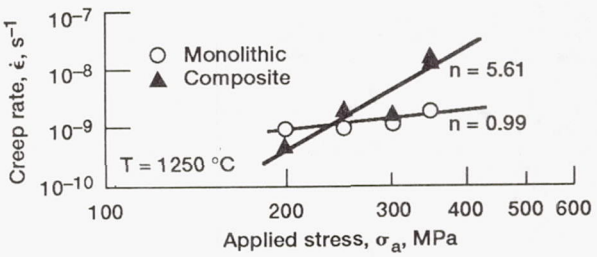

Figure 18.—Creep rate as a function of applied stress at 1250 °C.

REPORT DOCUMENTATION PAGE

Form Approved
OMB No. 0704-0188

1. AGENCY USE ONLY (*Leave blank*)	2. REPORT DATE	3. REPORT TYPE AND DATES COVERED
	December 1991	Technical Memorandum

4. TITLE AND SUBTITLE

Elevated Temperature Mechanical Behavior of Monolithic and SiC Whisker-Reinforced Silicon Nitrides

5. FUNDING NUMBERS

WU-505-63-1M

6. AUTHOR(S)

Jonathan A. Salem, Sung R. Choi, William A. Sanders, and Dennis S. Fox

7. PERFORMING ORGANIZATION NAME(S) AND ADDRESS(ES)

National Aeronautics and Space Administration
Lewis Research Center
Cleveland, Ohio 44135-3191

8. PERFORMING ORGANIZATION REPORT NUMBER

E-6572

9. SPONSORING/MONITORING AGENCY NAMES(S) AND ADDRESS(ES)

National Aeronautics and Space Administration
Washington, D.C. 20546-0001

10. SPONSORING/MONITORING AGENCY REPORT NUMBER

NASA TM-105245

11. SUPPLEMENTARY NOTES

Jonathan A. Salem and Dennis S. Fox, NASA Lewis Research Center; Sung R. Choi, Cleveland State University, Cleveland, Ohio 44115 and NASA Resident Research Associate at Lewis Research Center; William A. Sanders, Analex Corporation, 3001 Aerospace Parkway, Brook Park, Ohio 44142. Responsible person, Jonathan A. Salem, (216) 433-3313.

12a. DISTRIBUTION/AVAILABILITY STATEMENT

Unclassified - Unlimited
Subject Category 27

12b. DISTRIBUTION CODE

13. ABSTRACT (*Maximum 200 words*)

The mechanical behaviors of a 30 vol. % SiC whisker reinforced silicon nitride and a similar monolithic silicon nitride were measured at several temperatures. Measurements included strength, fracture toughness, crack growth resistance, dynamic fatigue susceptibility, post oxidation strength and creep rate. Strength controlling defects were determined with fractographic analysis. The addition of SiC whiskers to silicon nitride did not substantially improve the strength, fracture toughness, or crack growth resistance. However, the fatigue resistance, post oxidation strength and creep resistance were diminished by the whisker addition.

14. SUBJECT TERMS

SiC whisker reinforced silicon nitride; Strength; Toughness; Fatigue; Creep; Composite; Crack growth resistance

15. NUMBER OF PAGES

22

16. PRICE CODE

A03

17. SECURITY CLASSIFICATION OF REPORT	18. SECURITY CLASSIFICATION OF THIS PAGE	19. SECURITY CLASSIFICATION OF ABSTRACT	20. LIMITATION OF ABSTRACT
Unclassified	Unclassified	Unclassified	

NSN 7540-01-280-5500

Standard Form 298 (Rev. 2-89)
Prescribed by ANSI Std. Z39-18
298-102